Journal of Photochemistry & Photobiology A: Chemistry 364 (2018) 542–550

Contents lists available at ScienceDirect

Journal of Photochemistry & Photobiology A: Chemistry

journal homepage: www.elsevier.com/locate/jphotochem

Structural and optical properties of Cu-substitution of $NiAl_2O_4$ and their photocatalytic activity towards Congo red under solar light irradiation

F.Z Akika[a], M. Benamira[b,*], H. Lahmar[c], A. Tibera[a], R. Chabi[a], I. Avramova[d], Ş. Suzer[e], M. Trari[c]

[a] Laboratoire d'études des matériaux (LEM), Université de Jijel, BP. 98, Ouled Aissa, 18000 Jijel, Algeria
[b] Laboratory of Interaction Materials and Environment (LIME), University of Mohamed Seddik Ben Yahia, 18000 Jijel, Algeria
[c] Laboratory of Storage and Valorization of Renewable Energies, Faculty of Chemistry (USTHB), 16111 Algiers, Algeria
[d] Institute of General and Inorganic Chemistry, Bulgarian Academy of Sciences, Block 11, Acad. G. Bonchev Str., 1113 Sofia, Bulgaria
[e] Department of Chemistry, Bilkent University, Main campus, 068000 Ankara, Turkey

ARTICLE INFO

Keywords:
$Ni_{1-x}Cu_xAl_2O_4$X-ray diffraction
Photocatalysis
Congo red
Langmuir isotherm

ABSTRACT

The present work focuses on the effect of Cu substitution on the crystal structure and photocatalytic activity of nano-spinel oxides $Ni_{(1-x)}Cu_xAl_2O_4$ (x = 0.0–1.0). The synthesized compounds by co-precipitation route are characterized by X-ray diffraction, FT-IR, X-ray Photoelectron Spectroscopy, Scanning Electron Microscopy and UV–vis diffuse reflectance. The photocatalytic activity is followed by UV–vis spectroscopy and Electrochemical Impedance Spectroscopy in order to confirm the good performance of the catalyst and the charge separation of photogenerated (e^-/h^+) pairs. The photocatalytic efficiency of the synthesized catalysts is investigated through the decomposition of Congo Red dye under solar light irradiation. The efficient catalyst is $Ni_{0.2}Cu_{0.8}Al_2O_4$ with a removal conversion of 90.55% of the dye after 180 min. The parameters influencing the dye degradation like initial concentration are studied for the optimum degradation and the results have been discussed. This study shows that the adsorption kinetic of the Congo red has well followed the Langmuir isotherm model. The high photocatalytic activity of $Ni_{0.2}Cu_{0.8}Al_2O_4$ can be attributed to the valence band of the catalyst which enhances the mobility of the photoexcited charge carriers.

1. Introduction

Our earth needs urgent actions to save the environment from pollutant emissions such as heavy metals, organic compounds, pesticides, and dyes, generated by heavy manufacturing industries and complex technological activities. These environmental pollutants pose serious toxic risks to microorganisms and represent a threat to aquatic life and human beings [1–4].

In reality, large amounts of dyes generating specifically from activities such as printing in textile industries, leather tannery, chemical and food manufacture, as well as pharmaceutical industries are continuously introduced into the environment (water, soil, and air) without any control [5,6]. Despite the fact that they are considered the main pollutants, quantities of dangerous dyes produced worldwide through synthesis, treatment, and application are still released into the environment without any prior treatment [7]. Most of these dyes contain stable compounds and non-biodegradable which are difficult to be destroyed due to mesomeric effect [8]. In this context, Azo Congo red (CR) is cationic dye which contains one or more —N = N— groups with an aromatic structure and one of the most important and widely used dyes. Its degradation is essential and indispensable for ecological protection. In this respect, several techniques have been employed such as filtration, coagulation, adsorption, biological, and oxidation and advanced oxidation processes (AOPs).

However, these methods are costly and often become ineffective at low concentrations [9,10]. Recently, photocatalytic degradation of dyes through AOP under UV irradiation on semiconductors has received much attention mainly to its capacity to degrade numbers recalcitrant dyes [11–14]. Among the candidates, TiO_2, ZnS, ZnO, Fe_2O_3, WO_3 and CdS are semiconductors of choice which are widely used as photocatalysts, but they require sometimes expensive UV irradiation for photocatalysis owing to their large band gap (Eg). Recently metal sulphide with doped semiconductors and spinel magnetic nanoparticles is also used as photo-catalyst for the degradation of various dyes [15–17]. The use of visible light can be another alternative. On the other hand, other researchers have investigated the degradation of CR in presence of narrow bandgap semiconductors like the spinels [18–24].

It is convenient to note that the photocatalytic process is focused on the creation of an electron/hole (e^-/h^+) pairs by illumination with visible or UV light, depending on the nature of the semiconductor

* Corresponding author.
E-mail addresses: m_benamira@univ-jijel.dz, benamira18@yahoo.fr (M. Benamira).

https://doi.org/10.1016/j.jphotochem.2018.06.049
Received 28 December 2017; Received in revised form 29 June 2018; Accepted 29 June 2018
Available online 30 June 2018

($h\nu > E_g$). Both electrons and holes may migrate to the catalyst surface of semiconductors and with the presence of the adsorbed azo dyes, redox reactions take place. The oxidizing radicals could attack the azo dyes and convert them partially into CO_2, H_2O and nontoxic inorganic molecules [25,26]. In this regard, Comparelli et al. [26] reported that the formation of free radicals is essential to reduce absorbed dyes and act as oxidizing species.

The metal oxide semiconductor materials have been generated great interest for photolysis, photocatalytic, solid oxide fuel cells, and photovoltaic applications due to their optical, electrical, and optoelectronic properties [27–30]. The spinel aluminate materials are widely used as ceramic pigments, magnetic devices, refractory materials, and catalytic material for chemical reactions and they have been studied for their dielectric properties, chemical and thermal stability, as well as for their mechanical resistance [31–33]. The optical and fluorescence properties of these compounds are dependent on their particles size and preparation methods. The nano-spinel oxides, have received a great attention due to their catalytic properties but to our knowledge and according to the literature, no study in which $NiAl_2O_4$ doped with copper was found for the dyes degradation of azo dyes.

The present study reports the application of the spinel solid solutions $Ni_{(1-x)}Cu_xAl_2O_4$ (x = 0.0–1.0) type spinel as an efficient photocatalysts for the degradation under solar irradiation of Congo red, a recalcitrant azo dye. The effect of different parameters such as, initial RC concentration and catalyst dose has been examined and the results obtained are discussed. The model of the photocatalytic kinetics degradation has also been studied.

2. Materials and methods

2.1. Synthesis and characterization of catalysts

The chemicals used in this work were $CuCl_2.2H_2O$ 97% (Fluka AG), $Ni(NO_3)_2.6H_2O$ 97% (Sigma-Aldrich), $Al(NO_3)_3.9H_2O$ 98% (Biochem-Chemopharma). They were used without any further treatment. Nanopowder Copper doped Nickel Aluminates were prepared by co-precipitation method using nitrate salts (purity 98%) of Cu, Ni and Al and chelated by NaOH (4 N) as precursors. Congo red dye (molecular weight = 696.67 g/mol^{-1}, $C_{32}H_{24}N_6O_6S_2.2Na$) was used without any further treatment. The stock solution of CR was prepared by dissolving appropriate amount of CR in 1.0 L of distilled water. The working solutions were prepared by simple dilution with distilled water for the photocatalytic experiments.

Adequate quantities of precursor were dissolved in distilled water and magnetically stirred for a few minutes. The obtained solutions were diluted in order to adjust the solution pH. After, a solution of NaOH (4 N) was slowly added until the neutralisation where a chelate was obtained. The obtained precipitate was filtered and heated in air at 120 °C for 24 h. The resulting powders were ground and calcined at 300 °C for 8 h in order to remove the nitrates, then at 550 °C and 800 °C, respectively, for 5 h until the formation of fine powders.

The X-ray diffraction was carried out using Cu-K_α monochromatic radiation (λ = 1.54056 Å) of a D8 Advance Bruker diffractometer. Data were collected between 15° and 90° at 0.04°/step for a counting time of 5 s and analyzed by using JCPDS cards and the resulting patterns were indexed by comparison with standard XRD patterns. The Morphology and grain size of the powders were characterized by scanning electron microscope (SEM, ZEISS EVO40 model). The infrared spectra of samples, shaped as KBr pellets, were recorded in the range 450–4000 cm^{-1}, using a SHIMADZU 8400 s spectrometer. The UV–vis spectra were recorded using a JASCO V-670 spectrophotometer on the 200–1800 nm domain with MgO as a standard. X-ray Photoelectron Spectroscopy (XPS) measurements were performed using VG Escalab II electron instrument and Al Kα x-ray source under low pressure (10^{-7} Pa). The spectra were recorded at room temperature and calibrated against C 1 s line [34]. The C1 s, O1 s, Al2p, Cu2p, Ni2p, and photoelectron lines were recorded and corrected by subtraction of a Shirley-type background. [35].

2.2. Electrical, electrochemical and photocatalytic experiment

The electrical conductivity measurement was conducted using the two probe techniques [36] with a copper wire and silver paint. The polished pellet was introduced in a glass tube and isolated with resin epoxy. The electrochemical measurement was done at ambient temperature using a conventional three-electrode cell and potential was given against a saturated calomel electrode (SCE). The potential was swept at a scan rate of 5 mV s^{-1} and controlled by a Solartron Analytical 1287 A potentiostat. The Mott–Schottky plots of the interfacial capacitance were measured at a frequency of 10 kHz in 0.1 M Na_2SO_4 electrolyte. The electrochemical impedance spectroscopy (EIS) was done using a Solartron Analytical Frequency Response Analyzers (FRA) 1260 and the impedance spectra were recorded over a frequency range 100 kHz to 10 mHz with signal amplitude of 10 mV under the open circuit conditions. The Mott–Schottky and EIS measurements under illumination were done by using a xenon lamp (Phillips lamp, 150 W).

The photocatalytic tests were performed in a Pyrex cell. 50 mg of catalyst was suspended in 50 mL of RC aqueous solution (30 mg /L, pH ~7.2). The experimental measurements in dark were performed in a sealed black box. The amount of adsorbed RC is evaluated UV–visible spectrophotometer after the dark adsorption.

Before illumination, the solution with catalyst was stirred continuously in the dark for 60 min to establish the adsorption equilibrium of CR. Then, the reactor was exposed to solar light irradiation. The average solar light intensity at the midday measured with a Lux Meter was evaluated as 750 W/m^2, while the temperature averaged 30 °C.

At regular time intervals, the aliquots (about 4 mL) were drawn and centrifuged to remove the photocatalyst powders. The remaining RC concentration was determined with UV–visible spectrophotometer at λ_{max} = 498 nm (UV-1800 Shimadzu, Japan) and the RC degradation rate was calculated using the difference in the CR concentration in the aqueous solution before and after adsorption as:

$$\text{Degradation \%} = [1 - (A_t / A_0)] \times 100 \quad (1)$$

Where A_0 and A_t are the absorbance of RC solution at initial tile 0 and time (t), respectively. All the photocatalytic experiments were conducted during the months of May and June with direct exposure to sunlight.

3. Results and discussion

Fig. 1 shows the powder XRD patterns of $Ni_{(1-x)}Cu_xAl_2O_4$ (x = 0.0–1.0) obtained after calcination at 800 °C for 5 h in air. The samples were essentially pure and the patterns revealed single phases. All XRD peaks are indexed in a cubic spinel structure isotypic of $NiAl_2O_4$ (JCPDS, No 10-0339) cubic phase of space group Fd-3 m corresponding to the spinel structure. It should be noted that the XRD pattern of $NiAl_2O_4$ (x = 0.0) confirms the presence of impurity peaks attributed to NiO.

The Cu-substitution of $NiAl_2O_4$ in the Ni-site did not change the peak position, nevertheless the intensity of the peaks of the reflections (331) and (400) which corresponding to 38° and 45° of all the compositions does not evolve in the same way. The decrease of Cu content, corresponds to a continuously decrease of the peaks continuously. Indeed, these two peaks are very sensitive to the phenomenon of intensity inversion observed in the case of spinel structure [37]. Moreover, the intensity of the (422) peak increases with the increase of Ni^{2+} substitution by Cu^{2+}.

The lattice parameters obtained after Rietveld refinements using the Fullprof software (Table 1) increases with the increase of Cu content, due to the difference in ionic radii between Ni^{2+} and Cu^{2+} (r_{Cu2+}

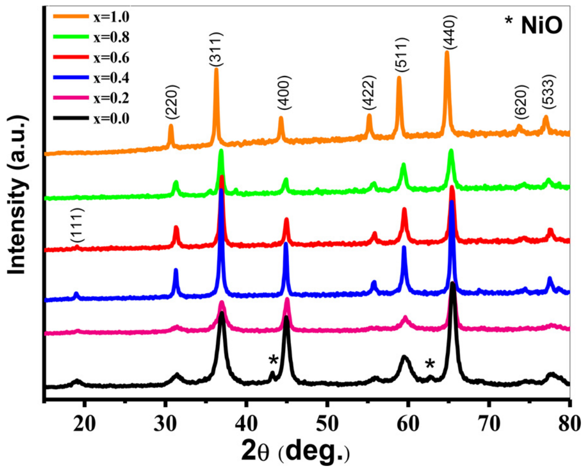

Fig. 1. Powder XRD patterns of $Ni_{(1-x)}Cu_xAl_2O_4$ oxides (x = 0.0–1.0) calcined at 800 °C.

Table 1
Refined structural parameters of $Ni_{(1-x)}Cu_xAl_2O_4$ powders (x = 0.0–1.0) synthesized through the co-precipitation route.

$Ni_{(1-x)}Cu_xAl_2O_4$	Crystallite size (nm)	Cell parameters a (Å)	χ^2	R_{wp}
x = 1.0	20.70	8.0692(1)	1.13	13.2
x = 0.8	17.41	8.0723(5)	1.19	13.0
x = 0.6	22.36	8.0595(3)	1.22	12.7
x = 0.4	19.15	8.0527(8)	1.33	13.3
x = 0.2	9.39	8.0533(2)	1.51	17.5
x = 0.0	8.80	8.0482(3)	1.41	15.2

(0.73 Å) > r_{Ni2+} (0.70 Å)) [38–40].

The radii values were taken from the Shannon Table for the ions in six fold coordination. The lattice parameters of $NiAl_2O_4$ and $CuAl_2O_4$ obtained in this study are in accordance with those reported in the literature [37,41,42].

The average crystallite size d_{DRX} is evaluated from the Debye-Scherrer equation:

$$d_{DRX} = \frac{0.9\,\lambda}{\beta\, cos\theta} \quad (2)$$

where β is the width at mid-height of the most intense peak (311) and θ is the diffraction angle.

The evolution of the crystallite size as a function of the copper content (Table 2) shows that the sizes vary between 8.8 and 22.4 nm confirming the obtention of nanometric crystallites.

The surface morphology of the obtained nanocrystals of $Ni_{(1-x)}Cu_xAl_2O_4$ was investigated by scanning electron microscopy (SEM). The obtained images (Fig. 2) confirm a polydispersed distribution of particles of nanometric sizes in the form of agglomerates. Consequently, the co-precipitation method allows obtaining nano crystallite.

Fig. 3 shows the FTIR spectra of the $Ni_{(1-x)}Cu_xAl_2O_4$ (x = 0.0–1.0) spinel powders recorded at room temperature between 450 and 4000 cm^{-1}. In general, all the spectra show the presence of broad absorption band around 3450 cm^{-1} characteristic of the adsorbed water and correspond to the stretching vibration of the hydroxyl group (ν

Table 2
Adsorption Parameters of the two isotherm models.

Langmuir		Freundlich	
Q max (mg/g)	5.81	1/n	1.58
K_l (L/mg)	0.366	K_f (L/mg)	1.190
R^2	0.992	R^2	0.887

(O—H)). While the band observed at 1644 cm $cm^{-1}$was attributed to the bending vibration of H—O—H. These values are in agreement with the literature [43,44]. The characteristic vibrational peaks of the spinel structure are observed between 500 and 800 (inset Fig.4). This can be associated with the vibrations of the tetrahedrally and octahedrally coordinated Al-O bond and the octahedrally coordinated Ni–O and Cu–O bands [34,41].

The XPS was employed to reveal the state for each element of the solid solution $Ni_{(1-x)}Cu_xAl_2O_4$ (x = 0.0–1.0) catalysts. The binding energies of the elements are reported separately in their regions for each composition (Fig. 4). All samples exhibit similar profiles in the O 1s spectral region with the presence of broad peaks of O 1 s at approximate binding energies of 530.5–531.09 eV (Fig. 4a). The peaks are ascribed to the characteristics of oxygen metal bonding in spinel oxides (oxygen of the lattice) including Cu—O, Ni—O and Al—O bonds according to the literature [45,46]. Fig. 4b reports the Al 2p region for all the samples; the binding energies for Al 2p peaks are in the range of 73.9–74.3 eV and characteristic of Al^{3+} environment [46].

Ni 2p region is characterized by two peaks at binding energies of 855.2–855.8 eV and 873.1–873.7 eV (Fig. 4c) with a shake-up peak at the high-energy side of the Ni $2p_{3/2}$ edge at around 862 eV [46–48], with a spin-orbital coupling around of 18.9 eV. This reveals the oxidation state of Ni^{2+} in all the samples in accordance with the literature, [46,48]. As shown in the spectrum, the intensities of the Ni $2p_{3/2}$ decrease when the Cu-content increases and disappears completely in $CuAl_2O_4$. Therefore, this situation suggests a harmonious substitution of Ni^{2+} by Cu^{2+}.

In the case of Cu 2p spectrum (Fig. 4d), the two pronounced peaks at about 932.9–934.6 eV and 952.8–954.6 eV resulting from spin-orbital coupling ($\Delta E \approx$ 20 eV) are assigned to Cu $2p_{3/2}$ and Cu $2p_{1/2}$ of Cu(II)/Cu(I), because it is so difficult to distinguish these states, whereas a broad shake-up peaks observed at around 941.5 and 963 eV can be assigned to the presence of Cu(II) [46,48,49]. Clearly, the intensities of Cu^{2+} peaks decrease when the Ni-content increases in the same manner in the Ni region which means that the surface is so rich with the cations (Ni, Cu and Al) for an eventual catalytic effect.

The values of the optical gap (Eg) of the as-prepared $Ni_{(1-x)}Cu_xAl_2O_4$ (x = 0.0–1.0) are determined from the measurement of the reflectance by UV–Vis diffused reflectance. The band gap can be determined by extrapolation to the energy axis of the linear plots $(\alpha h\nu)^n$ as a function of the photon energy ($h\nu$). To determine the type of transition, we have used the Tauc formula:

$$(\alpha h\nu)^m = A\,(h\nu - E_g) \quad (3)$$

Where α and A represent the absorption coefficient and a constant, respectively. The exponent m takes the value 2 for a direct transition and 1/2 for an indirect transition.

Fig. 5 illustrates an example of the UV–Vis diffused reflectance spectra obtained for x = 0.8 ($Ni_{0.2}Cu_{0.8}Al_2O_4$) and its direct band gap obtained from the plot of $(\alpha h\nu)^2$ versus $h\nu$. The direct optical band gap energy (E_g) for the as-prepared $Ni_{(1-x)}Cu_xAl_2O_4$ confirms a semiconductors character of the Cu-substituted $NiAl_2O_4$ compounds (Fig. 6).

The E_g values are found to decrease rapidly as x increases with Cu-substitution. This decrease can be attributed to the induced deep defects levels following the Cu doping. Therefore, the Cu-substituted $NiAl_2O_4$ can absorb more photons and generate more electron and holes, which is favorable for a higher photocatalytic activity compared to the unsubstituted compounds ($NiAl_2O_4$, $CuAl_2O_4$) with 2.37 and 2.04 eV of band gap energy (E_g), respectively. The E_g results agree with those reported in the literature for $NiAl_2O_4$ and $CuAl_2O_4$ [50–52].

The effect of contact time on the adsorption capacity of the CR onto $Ni_{(1-x)}Cu_xAl_2O_4$ (x = 0.0–1.0) catalysts is shown in Fig. 7a. As can be seen, the amount of adsorbed CR per unit weight of adsorbent (Qe) increases quickly at the beginning, except for the composition x = 0 ($NiAl_2O_4$), and remains nearly unchanged after 180 min, attesting the

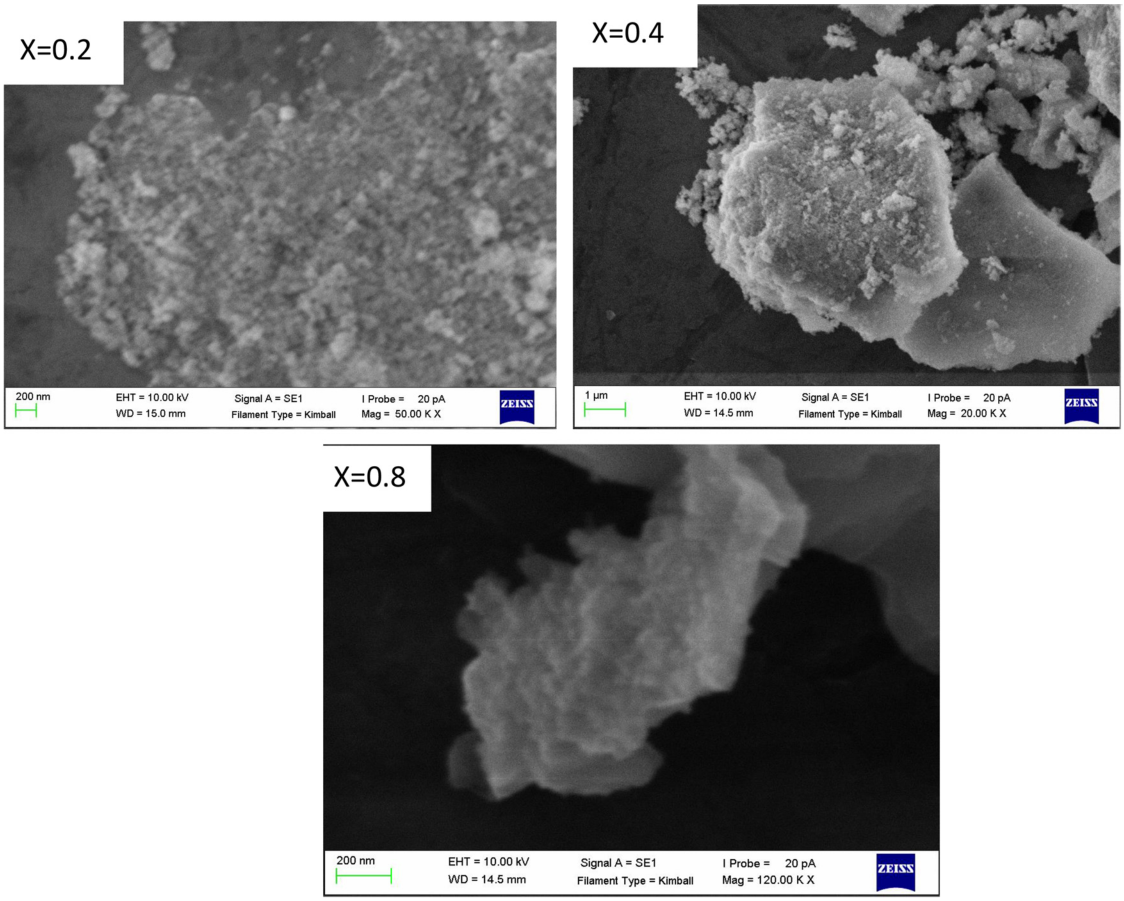

Fig. 2. SEM images of $Ni_{(1-x)}Cu_xAl_2O_4$ (x = 0.2 ; 0.4 et 0.8).

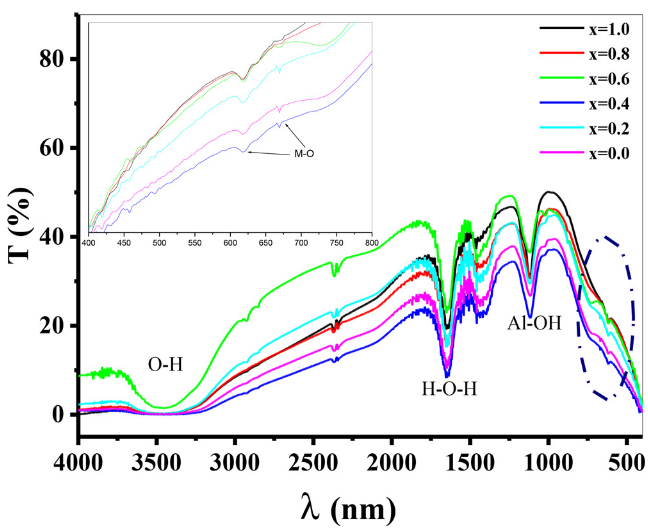

Fig. 3. FTIR spectra of $Ni_{(1-x)}Cu_xAl_2O_4$ oxides (x = 0.0–1.0) calcined at 800 °C.

equilibrium achievement. This is due to the large availability of free active sites on the surface of catalysts. The maximum adsorption capacity of CR adsorbed on adsorbent at equilibrium is obtained for x = 0.8 ($Ni_{0.2}Cu_{0.8}Al_2O_4$). This catalyst is used to study the photocatalytic activity for the rest of this work.

The effect of the initial CR concentration on the adsorption capacity of $Ni_{0.2}Cu_{0.8}Al_2O_4$ is shown in Fig. 7b. It is clear that the increase in the initial CR concentration from 0 to 40 mg/L results in an increase of the amount of CR adsorbed per unit weight of adsorbent (Qe), which reaches its maximum value for 15 mg/L. The excellent adsorption contributes to the increase of photocatalytic activity.

The Langmuir and Freundlich isotherm models were used to analyze the adsorption experimental data of CR on $Ni_{0.2}$ $Cu_{0.8}Al_2O_4$ catalyst (Fig. 8). The mathematical Langmuir and Freundlich equations are the following [53,54]:

$$\frac{C_e}{Q_e} = \frac{1}{Q_{max}\, k_l} + \frac{C_e}{Q_{max}} \quad (4)$$

$$\ln Q_e = \ln k_f + \frac{1}{n} C_e \quad (5)$$

where $Q_{\max}$ is the maximum adsorption capacity (mg g^{-1}), k_l is the Langmuir constant related to the energy of adsorption (L mg^{-1}), Ce is the CR equilibrium concentration (mg/L), K_f is the Freundlich constant related to the adsorption capacity of the adsorbent ($mg^{1-n}\,L^n\,g^{-1}$), and n is the constant related to the facility of adsorption process.

The obtained adsorption parameters are summarized in Table 2. The experimental data were obeyed and fitted much better with the Langmuir isotherm than with the Freundlich, indicating that the Langmuir model describes well the CR adsorption. The maximum adsorption capacity determined from Langmuir isotherm model was 5.81 mg/g not far from the experimental value obtained at equilibrium (Fig.7b). In addition, the result indicates that the adsorption process is mainly monomolecular layer on a catalyst surface.

The photocatalytic activity of $Ni_{0.2}Cu_{0.8}Al_2O_4$ catalyst has been investigated through the photodegradation of CR under solar light and the corresponding results are shown in Fig. 9a. The photocatalytic decolorization of CR solution in the absence of $Ni_{0.2}Cu_{0.8}Al_2O_4$ catalyst did not occur. In contrast, the decolorization is strongly improved in the presence of the catalyst. The photodegradation is quite slow at the

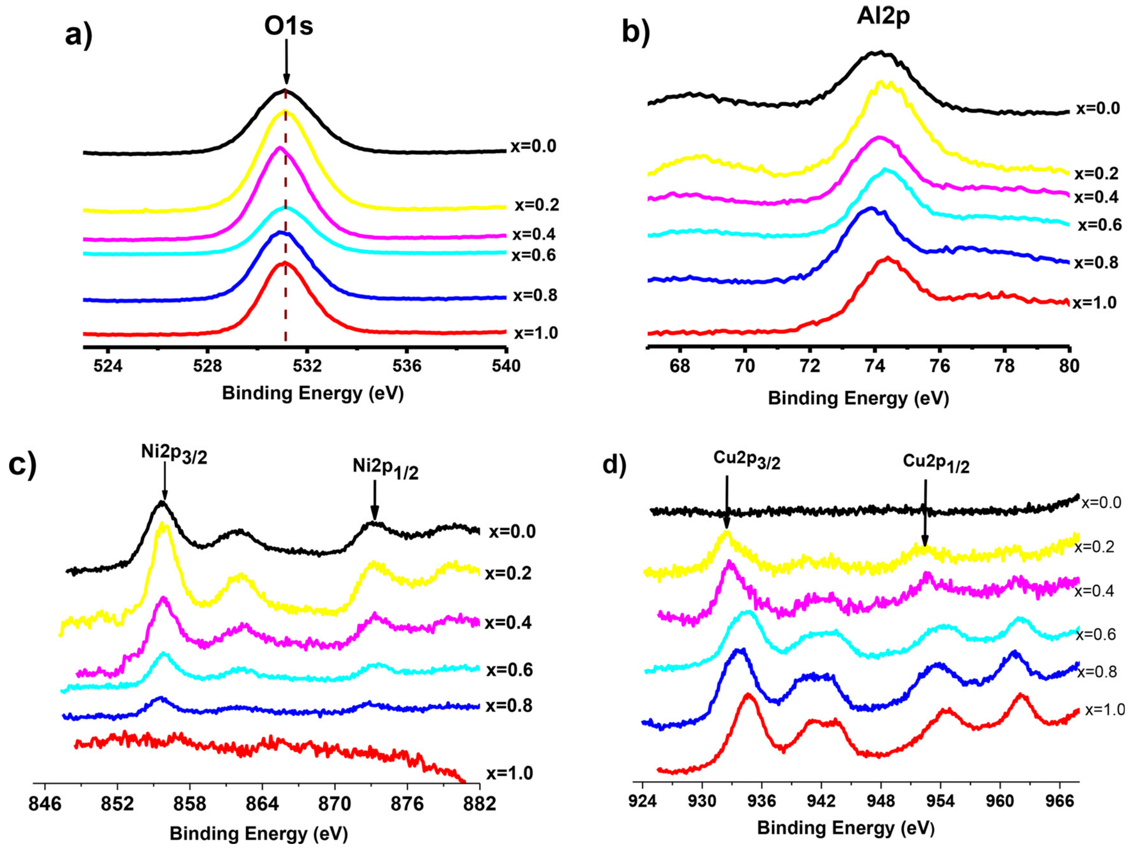

Fig. 4. XPS spectra of $Ni_{(1-x)}Cu_XAl_2O_4$ oxides (x = 0.0–1.0): (a) O 1 s, (b) Al 2p, (c) Ni 2p and (d) Cu 2p.

beginning and becomes faster after 50 min of exposure to solar light irradiation. The decolorization efficiency of 48% is obtained within 120 min which is better than commercial ZnO and TiO_2 P25 under UV light irradiation [30], 31% and 41%, respectively. 90.55% of CR was degraded after 180 min under solar light. This behavior can be attributed to the large surface area of the catalyst and electrons transfer, which facilitates the diffusion of CR molecules and retards the recombination of photogenerated electrons and holes (e^-/h^+) pairs.

In order to study the kinetics of the photodegradation of CR, the linear plots of the pseudo-first order kinetic model is used to fit the experimental data. The plots ln (C_0/C_t) vs. irradiation time are given in Fig. 9b. The linear relationship between ln(C_0/C) and irradiation time is given by the equation:

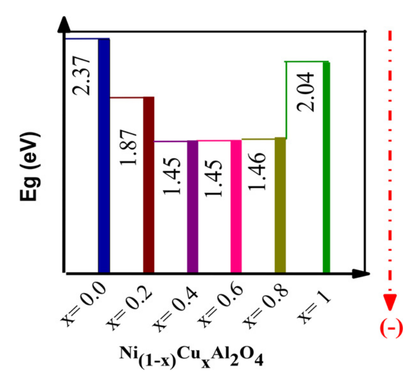

Fig. 6. Evolution of the band gap (Eg) as a function of x for $Ni_{(1-x)}Cu_xAl_2O_4$.

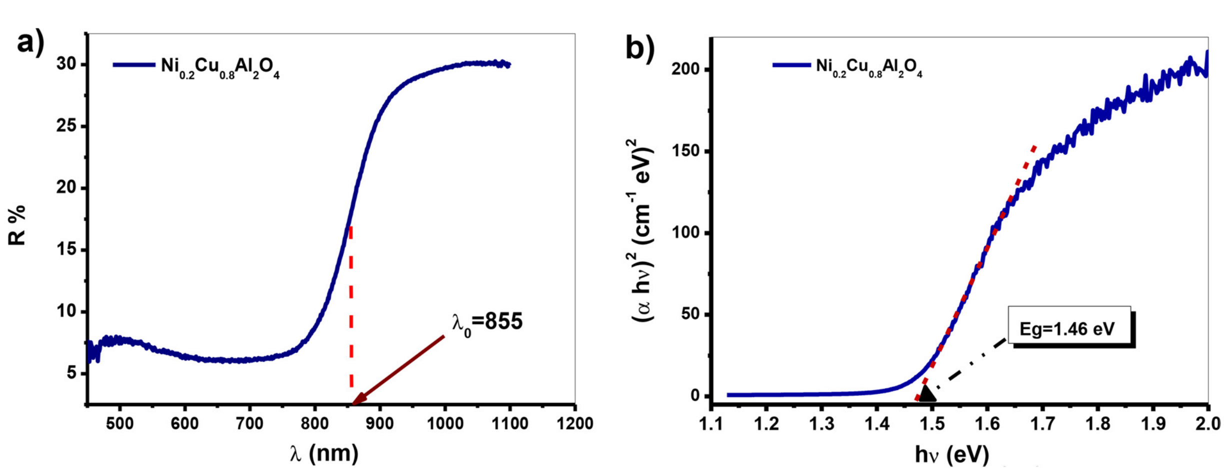

Fig. 5. (a) UV–Vis diffused reflectance spectrum of the as-prepared $Ni_{0.2}Cu_{0.8}Al_2O_4$ oxide, b) direct band gap estimation from the plot of $(\alpha h\nu)^2$ versus hν.

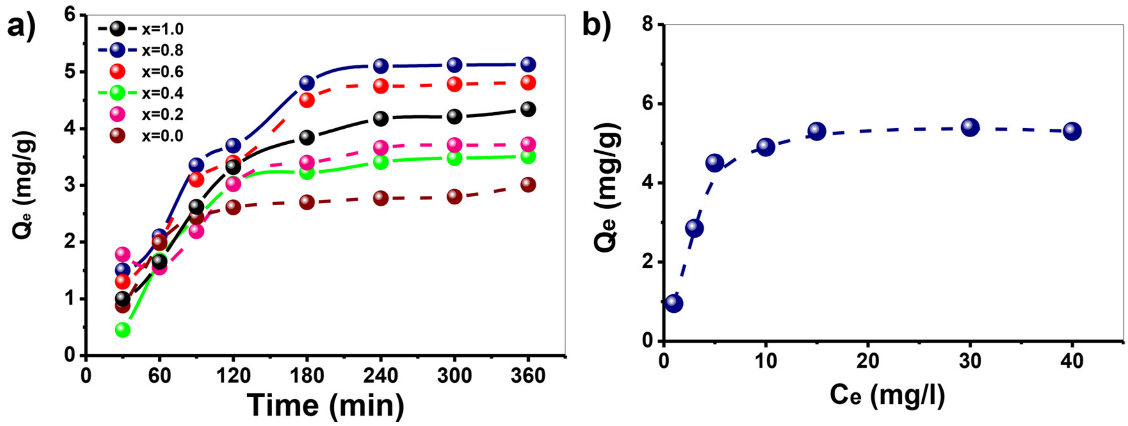

Fig. 7. a) Effect of contact time on the adsorption capacity of CR onto $Ni_{(1-x)}Cu_xAl_2O_4$ (x = 0.0–1.0) catalysts (initial [CR]: 30 mg L^{-1}; pH = 7.2), b) Effect of the initial CR concentration on the adsorption capacity of $Ni_{0.2}Cu_{0.8}Al_2O_4$.

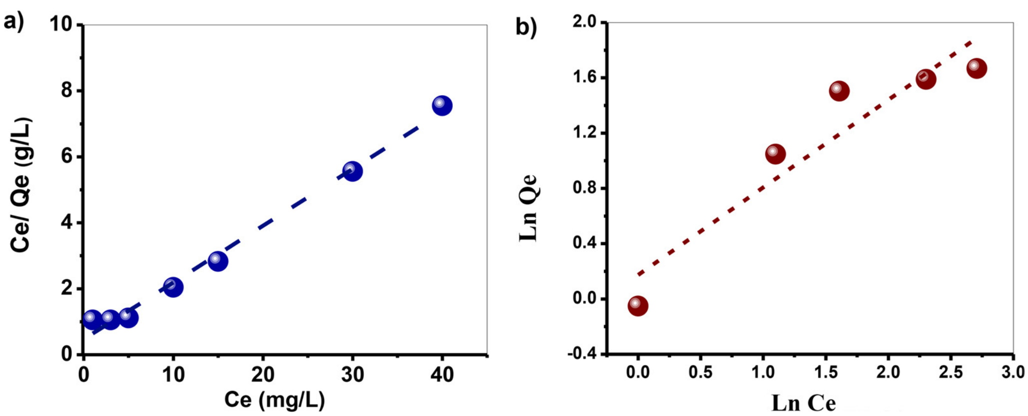

Fig. 8. Adsorption a) Langmuir and b) Freundlich isotherms of CR onto $Ni_{0.2}Cu_{0.8}Al_2O_4$.

$$\mathrm{Ln}\left(\frac{C_0}{C_t}\right) = k_{app}t \tag{6}$$

k_{app} (mn^{-1}) is the apparent rate constant, C_0/C_t is the normalized CR concentration and t is the reaction time. The value of the rate constant obtained is 0.004 min^{-1}.

The electrochemical impedance spectroscopy (EIS) is considered as the powerful technique to study the charge transfer at the solid / liquid interface. EIS is performed on the most efficient catalyst $Cu_{0.8}Ni_{0.2}Al_2O_4$ to confirm the charge separation of photogenerated (e^- / h^+) pairs [55,56]. Fig. 10 shows the Nyquist plots of the EIS spectra measured in the dark and under visible light irradiation for $Cu_{0.8}Ni_{0.2}Al_2O_4$ catalyst. The experimental data (symbol) suitably fit the calculated data (lines) using the equivalent circuit model (Fig. 10 insert). The error of the resistance (R) and Constant Phase Element (CPE) evaluated by the software Zview® is less than 1%.

The resistance at high frequency (R_1) is attributed to the electrolyte solution. The interface $Cu_{0.8}Ni_{0.2}Al_2O_4$/electrolyte behavior was characterised by one arc at medium and low frequencies and can be fitted by the resistance R_2 in parallel with the pseudo capacitance CPE attributed

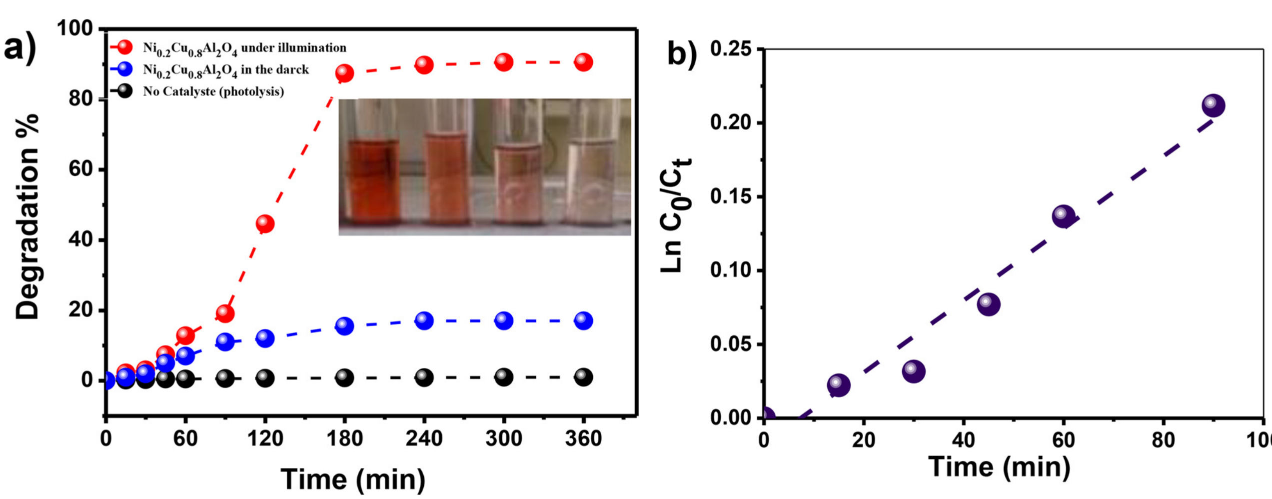

Fig. 9. Photodegradation activity of CR (30 mg L^{-1}) by the $Ni_{0.2}Cu_{0.8}Al_2O_4$ under solar light irradiation, b) the corresponding kinetics.

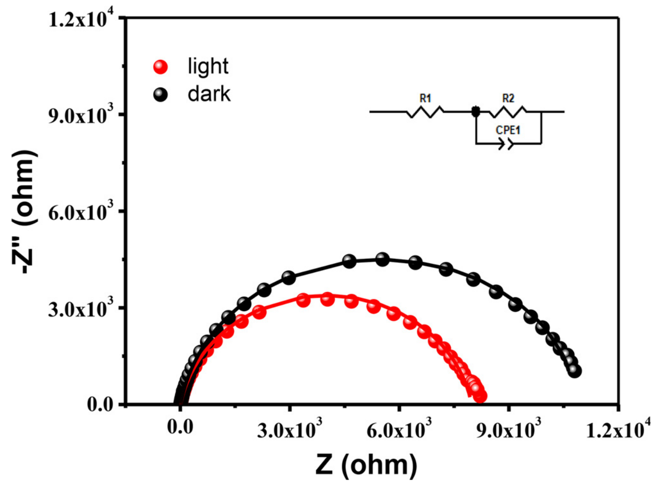

Fig. 10. EIS Nyquist plot of $Ni_{0.2}Cu_{0.8}Al_2O_4$ in the dark and under visible light irradiation measured in 0.1 M Na_2SO_4 aqueous solution.

to the double layer capacitance. R_2 is attributed to the charge transfer resistance and reflects the reaction rate occurring at the $Cu_{0.8}Ni_{0.2}Al_2O_4$ surface electrode. As expected, the resistance R_2 under visible light irradiation is smaller than that in dark which suggests a more effective separation of photo-generated (e^-/h^+) pairs and faster interfacial charge transfer at the solid–liquid interface highly desired for photocatalytic reaction [56,57].

The flat band potential (V_{fb}) used to predict the photocatalytic reactions is determined from the Mott-Schottky relation:

$$\frac{1}{C_{sc}^2} = \left(\frac{2}{e\varepsilon\varepsilon_o N_A}\right)(V - V_{bp}) \tag{7}$$

The extrapolated plot to $C^{-2} = 0$ gives the flat band potential $V_{fb}(-0.39\ V_{SCE})$ (Fig. 11a). The negative slope indicates a p-type semiconductor behavior.

The evolution of the electrical conductivity vs. 1000/T (Fig. 11b) shows that the electrical conductivity obeys to the Arrhenius law with activation energy (Ea) of 0.17 eV obtained from the slope and attributed to the separation between the Fermi level and the valence band. The valence band position of $Ni_{0.2}Cu_{0.8}Al_2O_4$ can be predicted using the known equation [58]:

$$E_{VB} = 4.75 + e\ V_{fb} + 0.059(pH - pH_{pzc}) + E_a \tag{8}$$

pH_{pzc} is the zeta potential determined by measuring the equilibrium pH of a solution containing an excess of $Ni_{0.2}Cu_{0.8}Al_2O_4$ powder ($pH_{pzc} = 7.20$). The photocatalytic mechanism on $Ni_{0.2}Cu_{0.8}Al_2O_4$ shows that both electrons and holes are involved in the CR degradation under solar light irradiation ($> E_g = 1.46$ eV). The photoelectrons produced in $Ni_{0.2}Cu_{0.8}Al_2O_4 - CB$ (1.68 V) were transferred to the surface and reduce the CR dye. The dissolved and/or adsorbed O_2 on the catalyst surface acting as the electron scavenger react with electrons and produce free radicals $\cdot O_2$ and $\cdot OH$ radicals (Fig. 12). Concomitantly, the holes react with H_2O to yield $\cdot OH$ radicals. The free radicals attack the adsorbed CR molecules on $Ni_{0.2}Cu_{0.8}Al_2O_4$. $OH\cdot$ radical is a very strong oxidizing agent with a standard potential +2.8 V [59] that can degrade CR to CO_2 and mineral end products. The relevant reactions at the surface of the interface catalyst can be expressed as follows:

$$Ni_{0.2}Cu_{0.8}Al_2O_4 + hv \rightarrow Ni_{0.2}Cu_{0.8}Al_2O_4\ (e^-_{CB} + h^+_{VB}) \tag{9}$$

$$Ni_{0.2}Cu_{0.8}Al_2O_4 + (h^+_{VB}) + H_2O \rightarrow Ni_{0.2}Cu_{0.8}Al_2O_4 + H^+ + OH^- \tag{10}$$

$$Ni_{0.2}Cu_{0.8}Al_2O_4 + (h^+_{VB}) + OH^- \rightarrow Ni_{0.2}Cu_{0.8}Al_2O_4 + \cdot OH \tag{11}$$

$$Ni_{0.2}Cu_{0.8}Al_2O_4 + (e^-_{CB}) + O_2 \rightarrow Ni_{0.2}Cu_{0.8}Al_2O_4 + O_2\cdot^- \tag{12}$$

$$O_2\cdot^- + H^+ \rightarrow HO2\cdot \tag{13}$$

$$\text{CR Dye} + OH\cdot\ /\ O_2\cdot^- \rightarrow CO_2 + H_2O + \text{other products nontoxic} \tag{14}$$

4. Conclusion

The results obtained in this study show that all spinel oxides $Ni_{(1-x)}Cu_xAl_2O_4$ (x = 0.0–1.0) prepared by co-precipitation route present a pure phase except the composition x = 0 which shows the presence of NiO confirmed by X-ray diffraction. The SEM images and UV–vis reflectance confirm that the samples have a nanometric size and a direct optical gap between 1.45 and 2.37 eV. The $Ni_{0.2}Cu_{0.8}Al_2O_4$ catalyst shows the best adsorption capacity of Congo red at natural pH with an equilibrium time of ∼3 h. The adsorption kinetics of CR dye obeys the Langmuir model on $Ni_{0.2}Cu_{0.8}Al_2O_4$.

The electrochemical study with EIS confirms the charge separation of photogenerated electrons and holes with good photocatalytic performance of the catalyst under solar light irradiation. The photocatalytic degradation of CR shows a removal of 90.55% of the dye after 3 h under illumination and the photodegradation follows the pseudo-first order kinetic model with a rate constant of 0.004 min^{-1}.

Acknowledgments

The authors are grateful to Dr. Himrane Mohamed for English improvement of the manuscript and Agence thématique de recherche en sciences et technologie (ATRST) for financial support (Projet de mobilité, NM2PHTE).

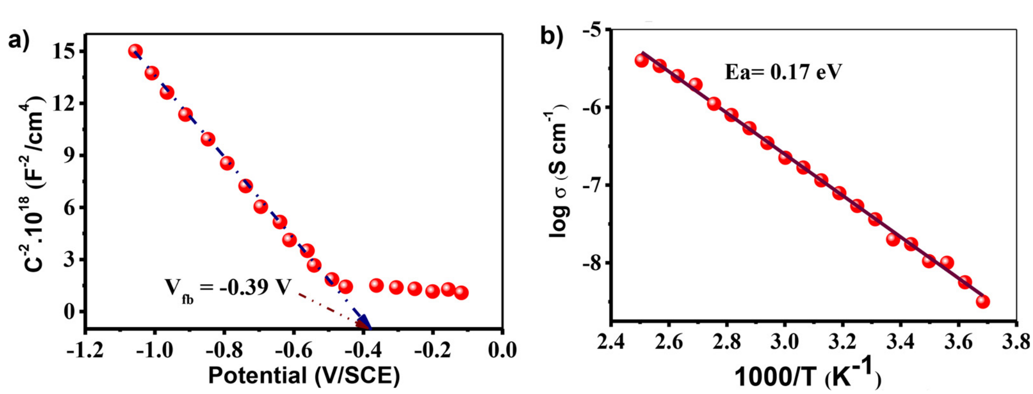

Fig. 11. a) The Mott Schottky plot at 10 kHz and b) The thermal variation of the electrical conductivity of $Ni_{0.2}Cu_{0.8}Al_2O_4$.

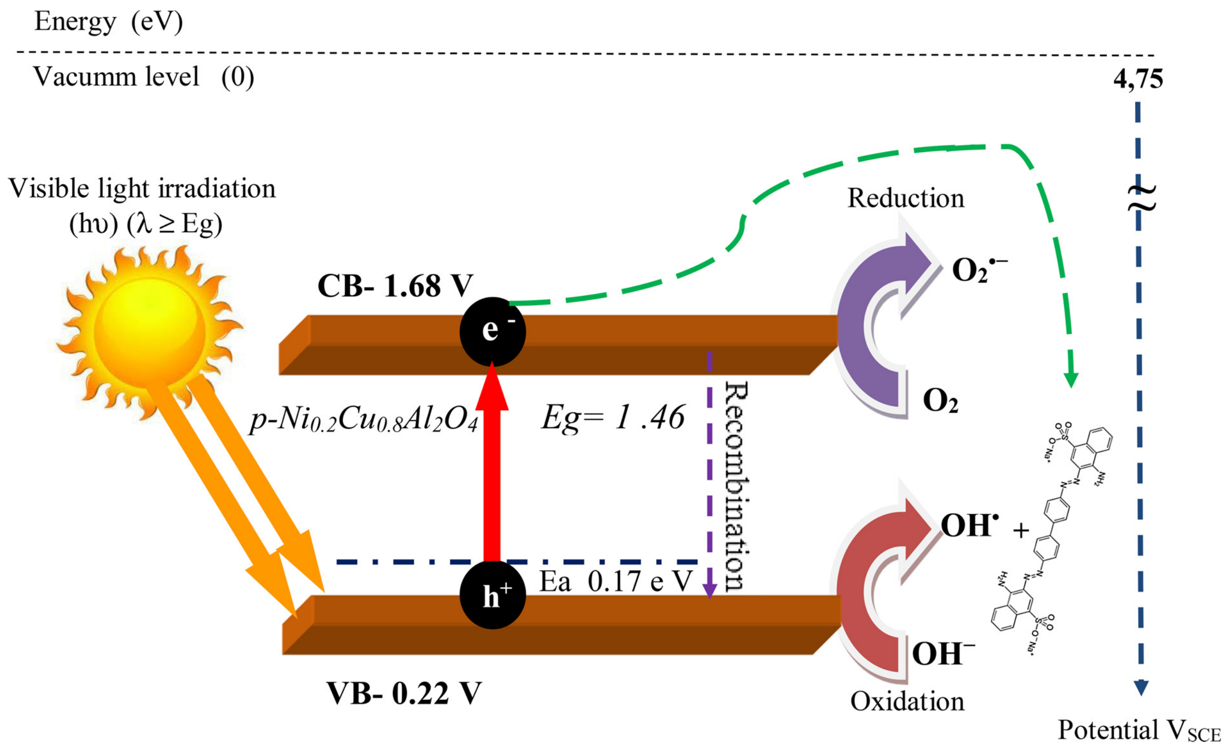

Fig. 12. A schematic illustration of the generation of electron-hole pairs and the corresponding redox reactions taking place on the $Ni_{0.2}Cu_{0.8}Al_2O_4$ surface.

References

[1] D.S. Bhatkhande, V.G. Pangarkar, A. Beenackers, Photocatalytic degradation for environmental applications - a review, J. Chem. Technol. Biotechnol. 77 (2002) 102–116, http://dx.doi.org/10.1002/jctb.532.

[2] P.B. Tchounwou, C.G. Yedjou, A.K. Patlolla, D.J. Sutton, Heavy Metal Toxicity and the Environment. Volume 3: Environmental Toxicology, in: Mol. Clin. Environ. Toxicol., 2012: pp. 133–164. doi:10.1007/978-3-7643-8340-4_6.

[3] N. Baliarsingh, K.M. Parida, G.C. Pradhan, Effects of Co, Ni, Cu, and Zn on photophysical and photocatalytic properties of carbonate intercalated MII/Cr LDHs for enhanced photodegradation of methyl orange, Ind. Eng. Chem. Res. 53 (2014) 3834–3841, http://dx.doi.org/10.1021/ie403769b.

[4] T. Robinson, G. Mcmullan, R. Marchant, P. Nigam, Remediation of dyes in textile e , uent : a critical review on current treatment technologies with a proposed alternative, Bioresour. Technol. 77 (2001) 247–255.

[5] B.H. Hameed, A.L. Ahmad, K.N.A. Latiff, Adsorption of basic dye (methylene blue) onto activated carbon prepared from rattan sawdust, Dye Pigment 75 (2007) 143–149, http://dx.doi.org/10.1016/j.dyepig.2006.05.039.

[6] W.C. Wanyonyi, J.M. Onyari, P.M. Shiundu, Adsorption of Congo red dye from aqueous solutions using roots of Eichhornia Crassipes: kinetic and equilibrium studies, Energy Procedia 50 (2014) 862–869, http://dx.doi.org/10.1016/J.EGYPRO.2014.06.105.

[7] I.A. Salem, Kinetics and mechanism of the color removal from congo red with hydrogen peroxide catalyzed by supported zirconium oxide, Transit. Met. Chem. 25 (2000) 599–604, http://dx.doi.org/10.1023/A:1007008808372.

[8] J. Fu, G.Z. Kyzas, Wet air oxidation for the decolorization of dye wastewater: an overview of the last two decades, Chin. J. Catal. 35 (2014) 1–7.

[9] E. Franciscon, M.J. Grossman, J.A.R. Paschoal, F.G.R. Reyes, L.R. Durrant, Decolorization and biodegradation of reactive sulfonated azo dyes by a newly isolated Brevibacterium sp. strain VN-15, Springerplus 1 (2012) 37.

[10] F. Kiriakidou, D.I. Kondarides, X.E. Verykios, The effect of operational parameters and TiO2-doping on the photocatalytic degradation of azo-dyes, Catal. Today 54 (1999) 119–130.

[11] A. Mokrini, D. Ousse, S. Esplugas, Oxidation of aromatic compounds with UV radiation/ozone/hydrogen peroxide, Water Sci. Technol. 35 (1997) 95–102.

[12] F. Wang, H. Yang, Y. Zhang, Enhanced photocatalytic performance of CuBi2O4 particles decorated with Ag nanowires, Mater. Sci. Semicond. Process. 73 (2018) 58–66.

[13] A. Afkhami, R. Moosavi, Adsorptive removal of Congo red, a carcinogenic textile dye, from aqueous solutions by maghemite nanoparticles, J. Hazard. Mater. 174 (2010) 398–403.

[14] G. Sivalingam, K. Nagaveni, M.S. Hegde, G. Madras, Photocatalytic degradation of various dyes by combustion synthesized nano anatase TiO2, Appl. Catal. B Environ. 45 (2003) 23–38.

[15] A. Sadollahkhani, Z.H. Ibupoto, S. Elhag, O. Nur, M. Willander, Photocatalytic properties of different morphologies of CuO for the degradation of Congo red organic dye, Ceram. Int. 40 (2014) 11311–11317.

[16] R. Bomila, S. Srinivasan, S. Gunasekaran, A. Manikandan, Enhanced photocatalytic degradation of methylene blue dye, opto-magnetic and antibacterial behaviour of pure and la-doped ZnO nanoparticles, J. Supercond. Nov. Magn. 31 (2018) 855–864.

[17] D. Maruthamani, S. Vadivel, M. Kumaravel, B. Saravanakumar, B. Paul, S.S. Dhar, A. Habibi-Yangjeh, A. Manikandan, G. Ramadoss, Fine cutting edge shaped Bi2O3rods/reduced graphene oxide (RGO) composite for supercapacitor and visible-light photocatalytic applications, J. Colloid Interface Sci. 498 (2017) 449–459.

[18] A.G. Abraham, A. Manikandan, E. Manikandan, S.K. Jaganathan, A. Baykal, P. Renganathan, Enhanced opto-magneto properties of Ni x Mg1−x Fe2O4 (0.0 ≤ x ≤ 1.0) ferrites nano-catalysts, J. Nanoelectron. Optoelectron. 12 (2017) 1326–1333.

[19] V.K. Jayaraman, A. Hernández-Gordillo, M. Bizarro, Importance of precursor type in fabricating ZnO thin films for photocatalytic applications, Mater. Sci. Semicond. Process. 75 (2018) 36–42.

[20] M. Sboui, M.F. Nsib, A. Rayes, T. Ochiai, A. Houas, Application of solar light for photocatalytic degradation of Congo red by a floating salicylic acid-modified TiO2/palm trunk photocatalyst, Comptes Rendus Chim. 20 (2017) 181–189.

[21] H. Guo, K. Lin, Z. Zheng, F. Xiao, S. Li, Sulfanilic acid-modified P25 TiO2 nanoparticles with improved photocatalytic degradation on Congo red under visible light, Dye Pigment 92 (2012) 1278–1284.

[22] H. Lachheb, E. Puzenat, A. Houas, M. Ksibi, E. Elaloui, C. Guillard, J.-M. Herrmann, Photocatalytic degradation of various types of dyes (Alizarin S, Crocein Orange G, Methyl Red, Congo Red, Methylene Blue) in water by UV-irradiated titania, Appl. Catal. B Environ. 39 (2002) 75–90.

[23] R.K. Wahi, W.Y. William, Y. Liu, M.L. Mejia, J.C. Falkner, W. Nolte, V.L. Colvin, Photodegradation of Congo Red catalyzed by nanosized TiO2, J. Mol. Catal. A Chem. 242 (2005) 48–56.

[24] H. Zhu, R. Jiang, L. Xiao, Y. Chang, Y. Guan, X. Li, G. Zeng, Photocatalytic decolorization and degradation of Congo Red on innovative crosslinked chitosan/nano-CdS composite catalyst under visible light irradiation, J. Hazard. Mater. 169 (2009) 933–940.

[25] K. Ullah, Z.-D. Meng, S. Ye, L. Zhu, W.-C. Oh, Synthesis and characterization of novel PbS–graphene/TiO2 composite with enhanced photocatalytic activity, J. Ind. Eng. Chem. 20 (2014) 1035–1042.

[26] R. Comparelli, E. Fanizza, M.L. Curri, P.D. Cozzoli, G. Mascolo, R. Passino, A. Agostiano, Photocatalytic degradation of azo dyes by organic-capped anatase TiO2 nanocrystals immobilized onto substrates, Appl. Catal. B Environ. 55 (2005) 81–91.

[27] A. Manikandan, E. Manikandan, B. Meenatchi, S. Vadivel, S.K. Jaganathan, R. Ladchumananandasivam, M. Henini, M. Maaza, J.S. Aanand, Rare earth element (REE) lanthanum doped zinc oxide (La: ZnO) nanomaterials: synthesis structural optical and antibacterial studies, J. Alloys Compd. 723 (2017) 1155–1161.

[28] E. Hema, A. Manikandan, P. Karthika, S.A. Antony, B.R. Venkatraman, A novel synthesis of Zn2+-doped CoFe2O4 spinel nanoparticles: structural, morphological, opto-magnetic and catalytic properties, J. Supercond. Nov. Magn. 28 (2015) 2539–2552.

[29] N.C.S. Selvam, A. Manikandan, L.J. Kennedy, J.J. Vijaya, Comparative investigation of zirconium oxide (ZrO2) nano and microstructures for structural, optical and photocatalytic properties, J. Colloid Interface Sci. 389 (2013) 91–98.

[30] S. Douafer, H. Lahmar, M. Benamira, G. Rekhila, M. Trari, Physical and photoelectrochemical properties of the spinel LiMn2O4 and its application in photocatalysis, J. Phys. Chem. Solids 118 (2018) 62–67.

[31] P. Bhavani, A. Manikandan, P. Paulraj, A. Dinesh, M. Durka, S.A. Antony, Okra (Abelmoschus esculentus) plant extract-assisted combustion synthesis and characterization studies of spinel ZnAl2O4 nano-catalysts, J. Nanosci. Nanotechnol. 18 (2018) 4072–4081.

[32] A. Manikandan, M. Durka, S.A. Antony, One-pot flash combustion synthesis, structural, morphological and opto-magnetic properties of spinel Mn x Co 1 − x Al 2 O 4 (x = 0, 0.3, and 0.5) nanocatalysts, J. Supercond. Nov. Magn. 28 (2015) 209–218.

[33] S. Suguna, S. Shankar, S.K. Jaganathan, A. Manikandan, Novel synthesis of spinel MnxCo1− xAl2O4 (x = 0.0 to 1.0) nanocatalysts: effect of Mn2+ doping on structural, morphological, and opto-magnetic properties, J. Supercond. Nov. Magn. 30 (2017) 691–699.

[34] T.L. Barr, S. Seal, K. Wozniak, J. Klinowski, ESCA studies of the coordination state of aluminium in oxide environments, J. Chem. Soc. Faraday Trans. 93 (1997) 181–186.

[35] D.A. Shirley, High-resolution X-ray photoemission spectrum of the valence bands of gold, Phys. Rev. B 5 (1972) 4709.

[36] H. Lahmar, M. Benamira, F.Z. Akika, M. Trari, Reduction of chromium (VI) on the hetero-system CuBi2O4/TiO2 under solar light, J. Phys. Chem. Solids 110 (2017) 254–259.

[37] C.O. Augustin, K. Hema, L.J. Berchmans, R. Kalai Selvan, R. Saraswathi, Effect of Ce4+ substitution on the structural, electrical and dielectric properties of NiAl2O4 spinel, Phys. Status Solidi 202 (2005) 1017–1024.

[38] S. Suguna, S. Shankar, S.K. Jaganathan, A. Manikandan, Novel synthesis and characterization studies of spinel Ni x Co1 − x Al2O4 (x = 0.0 to 1.0) nano-catalysts for the catalytic oxidation of benzyl alcohol, J. Nanosci. Nanotechnol. 18 (2018) 1019–1026.

[39] G. Padmapriya, A. Manikandan, V. Krishnasamy, S.K. Jaganathan, S.A. Antony, Spinel NixZn1− xFe2O4 (0.0 ≤ x ≤ 1.0) nano-photocatalysts: synthesis, characterization and photocatalytic degradation of methylene blue dye, J. Mol. Struct. 1119 (2016) 39–47.

[40] M. Han, Z. Wang, Y. Xu, R. Wu, S. Jiao, Y. Chen, S. Feng, Physical properties of MgAl2O4, CoAl2O4, NiAl2O4, CuAl2O4, and ZnAl2O4 spinels synthesized by a solution combustion method, Mater. Chem. Phys. 215 (2018) 251–258.

[41] M. Salavati-Niasari, F. Davar, M. Farhadi, Synthesis and characterization of spinel-type CuAl2O4 nanocrystalline by modified sol–gel method, J. Sol-Gel Sci. Technol. 51 (2009) 48–52.

[42] N. Sahli, C. Petit, A.-C. Roger, A. Kiennemann, S. Libs, M.M. Bettahar, Ni catalysts from NiAl2O4 spinel for CO2 reforming of methane, Catal. Today 113 (2006) 187–193.

[43] S. Lan, L. Liu, R. Li, Z. Leng, S. Gan, Hierarchical hollow structure ZnO: synthesis, characterization, and highly efficient adsorption/photocatalysis toward Congo red, Ind. Eng. Chem. Res. 53 (2014) 3131–3139.

[44] J. Yanyan, L. Jinggang, S. Xiaotao, N. Guiling, W. Chengyu, G. Xiumei, CuAl2O4 powder synthesis by sol-gel method and its photodegradation property under visible light irradiation, J. Sol-Gel Sci. Technol. 42 (2007) 41–45.

[45] B.A. Sexton, A.E. Hughes, T.W. Turney, An XPS and TPR study of the reduction of promoted cobalt-kieselguhr fischer-tropsch catalysts, J. Catal. 97 (1986) 390–406.

[46] B.V. Crist, Handbooks of monochromatic XPS spectra. vol. 2. Commercially pure binary oxides and a few common carbonates and hydroxides./Ed by BV Crist, XPS Int. LLC. (2005).

[47] X. Liu, L. Han, W. Liu, Y. Yang, Synthesis of Co/Ni unitary-or binary-doped CeO2 mesoporous nanospheres and their catalytic performance for CO oxidation, Eur. J. Inorg. Chem. 2014 (2014) 5370–5377.

[48] Y.S. Gong, C. Lee, C.K. Yang, Atomic force microscopy and raman spectroscopy studies on the oxidation of Cu thin films, J. Appl. Phys. 77 (1995) 5422–5425.

[49] F. Severino, J.L. Brito, J. Laine, J.L.G. Fierro, A.L. Agudo, Nature of copper active sites in the carbon monoxide oxidation on CuAl2O4and CuCr2O4Spinel type catalysts, J. Catal. 177 (1998) 82–95.

[50] I. Sebai, N. Salhi, G. Rekhila, M. Trari, Visible light induced H2 evolution on the spinel NiAl2O4 prepared by nitrate route, Int. J. Hydrogen Energy 42 (2017) 26652–26658.

[51] S.A. Hassanzadeh-Tabrizi, R. Pournajaf, A. Moradi-Faradonbeh, S. Sadeghinejad, Nanostructured CuAl2O4: Co-precipitation synthesis, optical and photocatalytic properties, Ceram. Int. 42 (2016) 14121–14125.

[52] M. Salavati-Niasari, F. Davar, M. Farhadi, Synthesis and characterization of spinel-type CuAl2O4 nanocrystalline by modified sol–gel method, J. Sol-Gel Sci. Technol. 51 (48) (2009).

[53] H. Lahmar, M. Kebir, N. Nasrallah, M. Trari, Photocatalytic reduction of Cr (VI) on the new hetero-system CuCr2O4/ZnO, J. Mol. Catal. A Chem. 353 (2012) 74–79.

[54] H. Zhao, H. Yu, X. Quan, S. Chen, H. Zhao, H. Wang, Atomic single layer graphitic-C 3 N 4: fabrication and its high photocatalytic performance under visible light irradiation, RSC Adv. 4 (2014) 624–628.

[55] W. Teng, X. Li, Q. Zhao, G. Chen, Fabrication of Ag/Ag 3 PO 4/TiO 2 heterostructure photoelectrodes for efficient decomposition of 2-chlorophenol under visible light irradiation, J. Mater. Chem. A 1 (2013) 9060–9068.

[56] Y. Bessekhouad, M. Trari, J.-P. Doumerc, CuMnO2, a novel hydrogen photoevolution catalyst, Int. J. Hydrogen Energy 28 (2003) 43–48.

[57] H.-Y. Zhu, R. Jiang, Y.-Q. Fu, R.-R. Li, J. Yao, S.-T. Jiang, Novel multifunctional NiFe2O4/ZnO hybrids for dye removal by adsorption, photocatalysis and magnetic separation, Appl. Surf. Sci. 369 (2016) 1–10.

[58] P. Sharma, N. Hussain, D.J. Borah, M.R. Das, Kinetics and adsorption behavior of the methyl blue at the graphene oxide/reduced graphene oxide nanosheet–water interface: a comparative study, J. Chem. Eng. Data 58 (2013) 3477–3488.

[59] A.J. Bard, R. Parsons, J. Jordan, Standard potentials in aqueous solutions, Int. Union Pure Appl. Chem. (1985) 834.